New constraints on biological production and mixing processes in the South China Sea from triple isotope composition of dissolved oxygen

Hana Jurikova[1], Osamu Abe[2], Fuh-Kwo Shiah[3], and Mao-Chang Liang[4]

[1]School of Earth and Environmental Sciences, University of St Andrews, KY16 9TS St Andrews, United Kingdom
[2]Graduate School of Environmental Studies, Nagoya University, 464-8601 Nagoya, Japan
[3]Research Center for Environmental Changes, Academia Sinica, 11529 Taipei, Taiwan
[4]Institute of Earth Sciences, Academia Sinica, 11529 Taipei, Taiwan

Correspondence to: Hana Jurikova (hj43@st-andrews.ac.uk) and Mao-Chang Liang (mcl@gate.sinica.edu.tw)

Abstract. The South China Sea (SCS) is the world's largest marginal sea, playing an important role in the regional biogeochemical cycling of carbon and oxygen. However, its overall metabolic balance, primary production rates, and their link to East Asian Monsoon forcing remain poorly constrained. Here, we report seasonal variations in triple oxygen isotope composition ($^{17}\Delta$) of dissolved O_2, a tracer for biological O_2, gross primary production (GP; inferred from $\delta^{17}O$ and $\delta^{18}O$ values), and net community production (NP; evaluated from oxygen–argon ratios) from the SouthEast Asian Time-series Study (SEATS) in SCS. Our results suggest rather stable mixed-layer mean GP rates of ~1500 $\pm$ 350 mg C m^{-2} d^{-1} and mean NP of ~−13 $\pm$ 20 mg C m^{-2} d^{-1} during the summer southwest monsoon season. These values indicate, within uncertainties and variabilities observed, that the metabolism of the system was in net balance. During months influenced by the stronger northeast monsoon forcing, the system appears to be more dynamic and with variable production rates, which may shift the metabolism to net autotrophy (with NP rates up to ~140 mg C m^{-2} d^{-1}). Furthermore, our data from the deeper regions show that SCS circulation is strongly affected by monsoon wind forcing, with a larger part of the water column down to at least 400 m depth fully exchanged during a winter, suggesting the $^{17}\Delta$ of deep O_2 as a valuable novel tracer for probing mixing processes. Altogether, our findings underscore the importance of monsoon intensity on shifting the carbon balance in this warm oligotrophic sea, and on driving the regional circulation pattern.

1 Introduction

The South China Sea (SCS) is the largest marginal sea of the world and significantly influences the regional biogeochemistry and climate (Wong et al. 2007a). The SCS also contributes to global circulation. A pathway through the SCS connects the tropical Pacific with the Indian Ocean impacting the Indonesian Throughflow, a current which plays a pivotal role in the coupled ocean and climate system (Qu et al., 2005). It has been suggested that marginal seas may act as a significant global atmospheric carbon dioxide sink (CO_2), primarily due to CO_2 absorption by continental shelf waters (Tsunogai et al., 1999; Liu et al., 2000; Yool and Fasham, 2001; Chen et al., 2003; Thomas et al., 2004). However, the heterogeneous nature together

with latitudinal differences between ocean margins makes joint extrapolations to a global scale highly uncertain. Most observations have revealed that seas at mid-latitude shelves, which experience strong spring blooms and clear seasonal patterns, function particularly well as CO_2 sinks (e.g. the North Sea (Frankignoulle and Borges, 2001); the Gulf of Biscay (Thomas et al., 2004); the Celtic Sea (Seguro et al., 2019); the East China Sea (Tsunogai et al., 1999; Wang et al., 2000) or the Middle Atlantic Bight (DeGrandpre et al., 2002)). Conversely, tropical and subtropical shelves and marginal seas, are most likely CO_2 sources (Cai and Dai, 2004) and a similar scenario may also be anticipated for the SCS. While several studies reaffirmed that the SCS indeed acts as a source of CO_2 to the atmosphere in the spring, summer and autumn (Rehder and Suess, 2001; Zhai et al., 2005) Tseng et al. (2005) reported on the uptake of CO_2 during winter from the SCS. The observed CO_2 invasion, driven by an unusual seasonal pattern in the oligotrophic open northern part of the SCS with elevated chlorophyll concentrations (0.30–0.35 mg m^{-3}) and primary production (300 mg C m^{-2} d^{-1}), was apparently large enough to compensate for the CO_2 evasion during the rest of the year, resulting in only minor net annual sea–atmosphere CO_2 fluxes (0.24 g C m^{-2} yr^{-1}; Tseng et al., 2007). Although the primary production and phytoplankton biomass are low for most of the year in the SCS, it appears that a clear winter maximum can be found regularly – a distinct seasonal pattern from other low latitude water bodies. Clearly, the role of the SCS, and marginal seas in general, is complex and their seasonal carbon cycling demands further study.

Owing to its geographical position between the Tibetan Plateau and the western Pacific warm pool, the SCS is continuously exposed to the East Asian Monsoon, which plays a fundamental role in its oceanography and biogeochemistry (see Wong et al., 2007a for an overview). From June to September, the weaker southwest summer monsoon (SWM) drives the anti-cyclonic circulation gyre, while the strong northeast winter monsoon (NEM) propels a basin-wide cyclonic circulation gyre between November and April (Fig. 1). This intense seasonal reversal drives the short- and long-term physical, chemical and biological processes that control the distribution of phytoplankton communities (Ning et al., 2004). As a result, intermediate chlorophyll a (Chl−a) concentrations are typically associated with the SWM, while the highest phytoplankton biomass is expected during the NEM due to increased diapycnal nutrient supply from the thermocline. Winter mean Chl−a concentrations often peak at about 0.50 mg m^{-3} in the subsurface chlorophyll maximum and at 0.20 mg m^{-3} at the surface (Liu et al., 2002). Upwelling produced by the convergence of currents in the cyclonic gyre near the Luzon Strait where the Kuroshio intrudes, can at times enhance the mean Chl−a concentration (to about 0.65 mg m^{-3}) and primary production in winter to about 8 times the summer values (Chen et al., 2006). Conversely, lowest Chl−a values have been observed during inter-monsoon seasons (Liu et al., 2002; Wong et al., 2007b; Li et al., 2017). Superimposed on the main seasonal monsoon-driven pattern, episodic events such as typhoons may temporarily elevate primary production due to wind-enhanced vertical mixing, bringing nutrients from the nutricline to the mixed layer and stimulating production. For instance, Lin et al. (2003) reported a bloom patch with average surface Chl−a concentrations of 3.20 ± 4.40 mg m^{-3} during the passing of a tropical cyclone Kai-Tak in July 2000. In addition to typhoons, the SCS has been suggested to be sensitive to various types of short-term physical forcings including tides, internal waves, eddies or topography-flow interactions. Generally, these tend to enhance vertical mixing, supplying nutrient-rich waters

2

Deleted: the
Deleted: on the other hand,
Deleted: due to their high annual surface temperatures and the absence of strong spring blooms
Deleted:). A
Deleted:),
Deleted: 3
Deleted: ;
Deleted: waters
Deleted: and
Deleted: the
Deleted: 5
Deleted: 2
Deleted: -
Deleted: 2
Deleted: 4

to the mixing layer, which enhance phytoplankton production and Chl-a concentration (to about 0.30–0.40 mg m^{-3}) in the oligotrophic waters of the SCS. Interannual variability in the SCS is primarily driven by the ENSO (El Niño–Southern Oscillation), which modulates the strength of the monsoon forcing, which in turn affects the regional marine biogeochemistry. During warm (cold) El Niño (La Niña) episodes in the Pacific, the monsoon tends to have a late (early) onset and the monsoon intensity is generally weaker (stronger; Zhou and Chan, 2007). Consequently, weakened wind mixing and strengthened water column stratification results in anomalously low Chl-a concentrations in the northern SCS. For example, the 1997–1998 El Niño event was one of the most powerful ENSO events in recorded history and caused concentration of surface Chl-a to drop from 0.20 to 0.10 mg m^{-3} in the northern SCS and the mean winter production to be reduced by about 40% (Shang et al., 2005; Tseng et al., 2009).

Accurate quantification of phytoplankton production rates, a fundamental property of the ocean system, remains a challenge primarily due to methodological biases. This has been a subject of increasing debate over the past years resulting in augmented efforts to compare and resolve production rates through different methods (e.g. Juranek and Quay, 2013; Regaudie-de-Gioux et al., 2014). In the SCS and at the SouthEast Asian Time-series Study (SEATS; Wong et al., 2007a) our understanding of primary production is predominantly limited to opportunistic assessments using the ^{14}C-assimilation method (Liu et al., 2002) or satellite-based SeaWiFS observations (Liu et al., 2002; Lin et al., 2003). While the traditional ^{14}C approach (Steeman-Nielsen, 1952) is limited due to its in vitro nature, which cannot reflect the time-averaged mixed-layer phytoplankton production (Marra, 2002), the latter relies on calibrations against field measurements that are spatially and temporally scarce (Carr et al., 2006). Although not exempt of uncertainties (Juranek and Quay, 2013), as these are inherent to any productivity determination, the triple oxygen isotope composition ($^{17}\Delta$) technique (Luz et al., 1999; Luz and Barkan, 2000) combined with O_2/Ar measurements has proved to be a powerful tool to provide a new perspective on evaluating primary production (e.g. Sarma et al., 2005; Reuer et al., 2007; Stanley et al., 2010; Hamme et al., 2012; Castro-Morales et al., 2013; Jurikova et al., 2016). The key advantage of this technique is that $^{17}\Delta$ allows for distinguishing photosynthetic O_2 input from other sources directly in situ, while the co-variation of $\delta^{17}O$ and $\delta^{18}O$, the "dual-delta approach" (Prokopenko et al., 2011; Kaiser, 2011), enables an estimation of the integrated gross productivity in the mixed layer.

In order to evaluate the photosynthetic O_2 production and its contribution to the local carbon balance as well as improve our understanding of seasonal variabilities in primary production in the SCS, we performed triple isotopic analyses and determined the O_2/Ar of dissolved O_2 samples from five vertical profiles during the occupation of SEATS in October 2013, August 2014 and April 2015. We combined the $^{17}\Delta$ and the O_2/Ar tracer to study the seasonal trends in photosynthetic vs. atmospheric O_2 input in the upper water column (~200 m), which we relate to the main monsoon seasons. Gross and net primary production rates are also estimated and discussed. Finally, owing to the limited contribution from photosynthesis and air-sea gas exchange to $^{17}\Delta$ signal in a parcel of deep water (200 to 3500 m), the potential for the application of the tracer for assessing mixing processes is discussed.

2 Methods

2.1 Sampling and analysis

Sampling was carried out aboard R/V OR-1 during cruises CR1053 (in October 2013), CR1084 (August 2014) and CR1103 (April 2015) at station 55 "SEATS" (the SouthEast Asian Time-series Study, 18° N, 116° E, Fig. 1) in the South China Sea (SCS). Seawater was collected using a rosette sampler equipped with 20-L Niskin bottles attached to a Seabird SBE 911 Plus CTD. Samples for dissolved oxygen analysis were obtained on October 16th in 2013 (11 depths: 5, 10, 30, 50, 80, 100, 150, 200, 300, 400 and 500 m), on August 5th (11 depths: 5, 10, 20, 80, 100, 200, 600, 1000, 1800, 2500 and 3500 m) and 6th in 2014 (13 depths: 5, 10, 20, 50, 80, 200, 400, 600, 1000, 1200, 1800, 2500 and 3500 m), and on April 24th (14 depths: 5, 10, 20, 80, 100, 150, 200, 300, 400, 500, 600, 1000, 1800 and 3500 m) and April 25th in 2015 (7 depths: 5, 10, 20, 30, 50, 80, 100; see also Supplement).

The accuracy of dissolved oxygen concentration measurements from the CTD was verified and calibrated against in vitro measurements. Briefly, water samples were siphoned into triplicate 60 ml bottles (Wheaton) and the Winkler titration method of Pai et al. (1993) was adopted for in vitro dissolved O_2 determination with a precision of 0.2 % r.s.d. (full scale). Concentrations of Chl–a were measured by a fluorometer (Chelsea AQUA tracka III) attached to the CTD to monitor vertical profiles of fluorescence, and calibrated by in situ Chl–a measurements with a Turner Designs fluorometer (10-AU-005) after extraction with 90% acetone using a non-acidification method (Gong et al., 1996). The precision of Chl–a measurements using a Turner fluorometer is usually better than 8 % for any chlorophyll values exceeding 0.50 mg m^{-3} (Strickland and Parsons, 1972), with any uncertainties on the estimation of Chl–a linked to the presence of Chl–b being below 5 %. (Lorenzen, 1981). We compared two mixed layer depth definitions; (1) temperature-based definition defined by 1 °C (ΔT) threshold from reference temperature value at 10 m depth, and (2) dissolved O_2-based definition defined by 1 % (ΔO_2) threshold from reference O_2 concentration at 10 m depth. Selected mixed layer depths were further verified by careful visual inspection of vertical temperature, density and dissolved oxygen profiles. Although the preferred dissolved O_2-based mixed layer definition considers a relative difference of 0.5 % O_2 concentration to a reference value at 10 m (Castro-Morales and Kaiser, 2012), we did not find this definition suitable for out study location, as the oscillations in O_2 concentration in the mixed layer alone were on the order of 0.5%. Instead, we opted for the 1 % definition which also closely agreed with the visual inspection of the profiles. The limit of the photic zone was defined as the depth where the photosynthetically active radiation (PAR) was 1 % of the surface value. We used Ocean Data View (ODV; Schlitzer, 2020) for profile visualisation.

Triple oxygen isotope analyses were carried out at Academia Sinica, Taiwan. The triple oxygen isotope composition, or ^{17}O-excess (Luz et al., 1999; Luz and Barkan, 2000) is defined as:

$$^{17}\Delta = [\ln(1 + \delta^{17}O) - \lambda \times \ln(1 + \delta^{18}O)], \tag{1}$$

4

where the isotopic compositions $\delta^{17}O$ and $\delta^{18}O$ represent the deviation of the abundance ratio of an isotopic and normal species in a sample relative to that of a standard:

$$\delta^* O = \left[(^*O/^{16}O)_{sample} / (^*O/^{16}O)_{standard} - 1 \right],\qquad(2)$$

where $^*O$ is either ^{17}O or ^{18}O. Here, $\delta^{17}O$ and $\delta^{18}O$ are expressed with respect to atmospheric air O_2, and following Luz and Barkan (2005) the factor λ is taken to be 0.518. As suggested by Luz and Barkan (2011), we note that a slope of $\lambda = 0.516$ might present a more appropriate choice. However, in order to enable a direct comparison to other studies, we preferred the earlier value, which has been largely applied in studies on marine production to date. The use of a slope $\lambda = 0.516$ would result in only a minor increase in $^{17}\Delta$ (about 1–8 % of the reported values), which for most of our samples remains within analytical uncertainties.

Our laboratory protocols for dissolved oxygen sample preparation and analysis are detailed in Jurikova et al. (2016). Note that O_2-Ar data is not available for the profile from October 2013 due to the setting of the gas chromatograph condition at a dry ice-acetone slush temperature for complete separation of O_2. In summary, dissolved gases were extracted from water following Emerson et al. (1995) and Luz et al. (2002). $\delta^{17}O$ and $\delta^{18}O$ of O_2 in the purified oxygen-argon mixture (or pure oxygen for October 2013 samples) were determined by dual inlet mass spectrometry (Thermo Scientific Finnigan MAT 253 IRMS). Similar as in Jurikova et al. (2016) an Ar correction was performed to correct for the distribution of gases between the headspace and water in the sampling flasks and normalised to air. A size correction for the total amount of gas in the sample was not required at our current mass spectrometer setting and hence not applied. This was tested by the measurement of air samples and a working reference at varying gas concentrations, ranging approximately 20 to 60 µmol of O_2-Ar mixture. The reduction of sample size by a factor of ~2 did not affect the measured ratios, with the standard deviation between the air samples (n = 8) being ±0.36 ‰, ±0.070 ‰, ±1 per meg, and ±9 ‰ for $\delta^{17}O$, $\delta^{18}O$, $^{17}\Delta$, and $\delta(O_2/Ar)$, respectively (see Supplement). Potential fractionation of the working reference gas in the bellow during analysis (also known as the 'bleed effect'; see also Mahata et al., 2012) was monitored by noting the change in oxygen isotope ratios throughout the analysis (in the range of 100 to 20% of the bellow capacity). Based on one year of analyses (more than 20 batches measured, with one batch consisting typically of 12 measurements against the same working reference aliquot in the bellow) we found the bleed effect to be small and corrected. The bleed effect on $\delta^{18}O$ was ~0.15–0.20 ‰ per 10 sample analyses (~20 hours of mass spectrometer time) and <10 per meg for $^{17}\Delta$. To minimise any potential bleed effects, a limited number of sample analyses only was performed for each reference gas refill. To monitor the bleed effect, 2–3 atmospheric air samples were analysed alongside dissolved O_2 samples in each batch (against the same working reference aliquot), with no significant fractionation observed. Overall, our actual and long-term precision (1σ, standard deviation) established from routine measurements (n = 36)

Deleted: prefer

Deleted: The

Deleted: –

Deleted: profile

Deleted: in

Deleted: from

Deleted: Our

of atmospheric air O_2 was 0.017 ‰, 0.030 ‰, and 6 per meg for $\delta^{17}O$, $\delta^{18}O$, and $^{17}\Delta$, respectively, and our O_2 scale (Jurikova

et al., 2016; Liang and Mahata, 2015; Liang et al., 2017) is in agreement with that of Luz and Barkan (2011). The O_2/Ar ratio

215   was obtained by peak jumping following Barkan and Luz (2003), and is expressed as $\delta(O_2/Ar)$ (‰) =

$[(32/40)_{sample}/(32/40)_{standard} - 1] \times 10^3$. The long-term precision (1σ) of routine measurements of atmospheric air was better

than 5 ‰. Results from the equilibrated water samples (n = 3, 1σ) gave a mean $^{17}\Delta_{eq} = 11 \pm 3$ per meg, $\delta^{17}O_{eq} = 0.323 \pm 0.020$

‰, $\delta^{18}O_{eq} = 0.603 \pm 0.037$ ‰, and $\delta(O_2/Ar)_{eq} = -102 \pm 4$ ‰ (Jurikova et al., 2016).

2.2 Primary production calculations

220   To quantify gross production rates from $\delta^{17}O$ and $\delta^{18}O$ values we followed the standard "dual-delta approach" following

Prokopenko et al. (2011) and Kaiser (2011), where the gross oxygen production (GOP) may be calculated as follows:

$$GOP = KC_o \left[\frac{\left(1 - \frac{1+\delta^{17}O_{eq}}{1+\delta^{17}O}\right) - 0.518\left(1 - \frac{1+\delta^{18}O_{eq}}{1+\delta^{18}O}\right)}{\left(\frac{1+\delta^{17}O_p}{1+\delta^{17}O} - 1\right) - 0.518\left(\frac{1+\delta^{18}O_p}{1+\delta^{18}O} - 1\right)} \right], \tag{3}$$

225   where δ^*O is the measured value in a sample, δ^*O_{eq} is the relative abundance between air O_2 and dissolved O_2 in equilibrium

with the atmosphere (i.e. the results from the equilibrated water samples, Section 2.1; Jurikova et al., 2016), and δ^*O_p represents

the photosynthetic O_2 (Luz and Barkan, 2011). C_o is the O_2 concentration at saturation using solubility coefficients from Benson

and Krause (1984) and K is the piston velocity, the coefficient for gas exchange. K was calculated using the quadratic

relationship appropriate for wind speeds between 3 and 15 m s^{-1} (K = 0.24 × U_{10}^2 × (Sc/660)$^{-0.5}$) and normalised to Schmidt

230   number 660 (Sc$_{660}$) based on mixed layer temperatures (Wanninkhof et al., 2009). We compared two different approaches for

deriving K. The resulting K values are available in Table 1. First, we used a simple approach where K was derived from mean

NCEP wind speeds (Fig. 2) and averaged over the O_2 residence time in the mixed-layer preceding sampling (K$_{avg}$; 12, 5.6, and

4.4 days for October 2013, August 2014 and April 2015, respectively), based on the average mixed-layer depth and the gas

transfer coefficient. Second, we used the approach of Reuer et al. (2007) where K was calculated using a weighting technique,

235   which considers variable wind speeds and accounts for the fraction of mixed layer ventilated each day (K$_{wgh}$). For this, K was

derived from satellite wind speed measurements of hourly resolution using the ERA5 dataset (ECMWF, European Centre for

Medium-Range Weather Forecasts, https://www.ecmwf.int/; Supplement). Following Reuer et al. (2007), the fraction of the

mixed layer ventilated on the collection date (f$_1$) was determined from the mixed layer depth (Z$_{MLD}$) and gas transfer velocity

on the collection day (K$_1$) as f$_1$ = K$_1$ × 1day/Z$_{MLD}$, and was assigned a weight ω$_1$ = 1. The fraction of the mixed layer ventilated

240   prior to the sample collection day (day 2) was similarly calculated as f$_2$ = K$_2$ × 1day/Z$_{MLD}$, but was assigned a reduced weight

according to the fraction of the mixed layer ventilated on day 1 (ω$_2$ = ω$_1$ × (1–f$_1$)). Since the SEATS station was occupied for

a limited time only during each cruise, we used the Z$_{MLD}$ of the collection date for all calculations. Considering the rather

regular interannual pattern and minimal daily variations in the mixed layer depth, the used mean value should be a suitable

representation for the different sampling months (see also Section 3.1). The weight on the tth day prior to the sampling is described by the general term $\omega_t = \omega_{t-1} \times (1- f_t)$. A weighted gas transfer velocity for each day was then calculated as $K_t \omega_t$, and the weighted gas exchange rate for the mixed layer as:

$$K_{wgh} = \frac{\Sigma_{t=1}^{30} K_t \omega_t}{(1-\omega_{30}) \Sigma_{t=1}^{60} \omega_t} \tag{4}$$

where the term $(1-\omega_{30})$ accounts for the residual unventilated portion of the mixed layer. We utilised 30 days for each sampling date (October 2013, August 2014 and April 2015) as the residual fraction on the 30th day was already minimal. The two approaches for deriving K resulted in different production rates, with the K_{avg} either underestimating or overestimating production when compared to K_{wgh}, by ~38 % in October 2013, ~47 % in August 2014, and ~21 % in April 2015 (this applies to both gross and net production rates since the choice of K affects both proportionally). We therefore used K_{wgh} for calculating production rates at SEATS.

Mixed-layer O_2 production time (O_2 concentration in the mixed layer/O_2 gross production rate) was determined to evaluate the rate at which O_2 was produced biologically against the physical O_2 residence time. The O_2 production time was estimated from the measured O_2 concentrations and the GOP and was generally lower than the O_2 residence time (0.3 days for October 2013, 1.3 and 1.4 days for August 5th and 6th 2014, respectively, and 1.0 and 3.6 days for April 24th and 25th 2015, respectively).

To assess the net oxygen production rates (NOP), we used the O_2/Ar measurements consistent with the biological O_2 supersaturation concept for net photosynthetic production. Because the physical properties of O_2 and Ar are similar, and Ar has no biological sources and sinks, measurements of Ar concentration in water may be used to remove physical contributions to O_2 supersaturation. The biological oxygen supersaturation $\Delta(O_2/Ar)$ (given in %) is defined as the relative deviation of the O_2/Ar in a sample to the O_2/Ar at equilibrium with the atmosphere (e.g. Craig and Hayward, 1987; Emerson et al., 1995; Kaiser et al., 2005) and may be calculated as follows:

$$\Delta(O_2/Ar) = \left[\frac{1+\delta(O_2/Ar)_{sample}}{1+\delta(O_2/Ar)_{eq}} - 1 \right], \tag{4}$$

NOP can be calculated from $\Delta(O_2/Ar)$ values following Luz et al. (2002):

$$NOP = K \times C_o \times [\Delta(O_2/Ar)]. \tag{5}$$

The estimation of both GOP and NOP via the presented approaches relies on the assumption that the mixed layer is at a steady state, and that there is no significant entrainment or upwelling of low-O_2 subsurface water into the mixed layer, nor lateral advection from adjacent waters.

Production rates were converted from O_2 to C units following a commonly applied approach (e.g., Hendricks et al., 2014; Juranek et al., 2012). To scale GOP to gross C production, we accounted for the fraction of O_2 linked to Mehler reaction and photorespiration following Laws et al. (2000) by applying a photosynthetic quotient (PQ) of 1.2. For NOP conversion we used a PQ of 1.4 for new production (Laws, 1991). Hereinafter, we refer to the scaled production rates in C units as GP and NP.

3 Results

3.1 Oceanographic setting

Vertical distribution of physical parameters, chlorophyll and dissolved O_2 composition were measured from profiles collected at SEATS during October 2013, August 2014 and April 2015. Generally, during the sampling campaigns the temperature-based mixed layer (see Section 2.1 for definition) variations were only minor and varied depending on the month. Highest surface temperatures of 29 °C were recorded during the summer in August 2014. In October 2013, the surface temperature was 28 °C. Lowest surface temperature of 27 °C was observed in April 2015. Temperature-based mixed layer depth limit was deepest at 49 m on the 16th of October 2013. In August 2014, the mixed layer was relatively shallow, but changed from 25 m on the 5th to 34 m on the 6th. In April 2015, the mixed layer depth limit was 28 m and 26 m on the 24th and 25th, respectively (Table 1). The dissolved O_2-based mixed layer definition resulted in mixed layer depths of 48 m on the 16th of October 2013, 20 m and 32 m on the 5th and 6th August 2014, and 27 m and 25 m on the 24th and 25th April 2015, respectively (Table 1). The mixed layer depths determined by the different criteria were in close agreement within 2 m, except for on the 5th August 2014 when the difference between the definitions was 5 m. As the O_2-based definition was more conservative and is directly related to the species of interest of this study, we used the O_2-based mixed layer depths for estimating integrated mixed layer production from the isotopic composition of dissolved O_2.

The observed mixed layer depths and interannual pattern fit well within the trend expected for SEATS, which appears to stay rather regular between years (Wong et al., 2007; Tai et al., 2017). A shallow mixed layer (about 20 m deep in summer and up to 100 m in winter) and a persistent stratification throughout the year are characteristic features of SEATS. The average maximum mixed layer depth at SEATS is ~80 m occurring in December and January. Throughout spring, the mixed layer depth steadily decreases reaching minimum ~25 m in May. Afterwards, the mixed layer increases again gradually reaching ~35 in June and remains approximately constant through to October, after which it increases sharply to reach its maximum winter values (Tai et al., 2017).

8

The chlorophyll fluorescence was generally low and restricted to the thermocline in the upper 50−100 m (Fig. 3), as expected
for the oligotrophic northern SCS (see Section 1), with the absolute magnitude of the subsurface maximum peak varying
between seasons. Interestingly, Chl−a was highest of 0.60 mg m^{-3} in October 2013 (Fig. 3a). In August 2014 the concentration
remained at $0.20-0.30$ mg m^{-3} without pronounced variations and diurnal trends (Fig. 3b). In April 2015, we observed a minor
increase in the subsurface chlorophyll maximum, but mostly restricted to the dawn hours, of up to 0.50 mg m^{-3}, which gradually
declined throughout the day and was lowest at night of approximately 0.20 mg m^{-3} (Fig. 3c).

The dissolved O_2 saturation in the upper 400 m on the different sampling days is shown in Figure 3d. In October 2013, the
mixed layer was saturated between 100 % and 102 %, and below in the thermocline the O_2 saturation decreased. In August
2014, the O_2 was saturated throughout the mixed layer (100 %) on the first collection day, and between 97–98 % on the second
day. In April 2015, the mixed layer O_2 saturation hovered between 97–98 % on the first day, and 102–103 % on the second
day. Below the limit of the mixed layer O_2 saturation increased by few % on both days in August 2014 as well as on 24th April
2015. A more prominent supersaturated O_2 peak reaching 110 % below the mixed layer was observed on April 25th 2015.

Based on our sampling months and the observed physical parameters, the profile from October 2013 appears to reflect the
transition from summer to winter conditions. The lack of basin-wide prevailing monsoon forcing is also evident from surface
wind maps (Fig. 2a), indicating that this collection date might largely represent an inter-monsoon period. The shallow mixed
layer in August 2014 and southwest wind direction point towards typical summer monsoon conditions (Fig. 2b). Conversely,
the mixed layer characteristics in April 2015 are suggestive of spring conditions, although the surface wind maps still indicate
the presence of the northeast winter monsoon in the area (Fig. 2c). We therefore conclude that the April 2015 collection days
likely reflect late northeast (winter) monsoon season during spring.

3.2 Dissolved O_2 composition: $^{17}\Delta$ and $\Delta(O_2/Ar)$

The triple isotope composition of dissolved O_2 profiles from SEATS is shown in Figure 4. We observed broad variations in
both the $^{17}\Delta$ and the $\Delta(O_2/Ar)$ between the different months as well as the days when the samples were collected, overall
ranging between 22 and 229 per meg and −72 to 2.2 %, respectively. At large, the upper ocean $^{17}\Delta$ profiles outlined a common
trend, with lower $^{17}\Delta$ in the mixed layer, a peak in the values below, and a gradual decrease towards 200 m depth. The average
mixed layer values (Table 1), and the depth of the $^{17}\Delta$ maximum peak as well as its magnitude, however, varied considerably
between months and collection days. Highest mixed layer $^{17}\Delta$ values averaging 90 ± 28 per meg were observed in October
2013. On August 5th and 6th 2014 and April 24th 2015 the O_2 compositions were comparable yielding mean mixed layer $^{17}\Delta$
values of 59 ± 9, 54 ± 18 and 52 ± 11 per meg, and $\Delta(O_2/Ar)$ values of -0.3 ± 0.5, -0.2 ± 0.2, and -0.5 ± 3.5 %, respectively.
Lowest mixed layer $^{17}\Delta$ values of 26 ± 5 per meg with positive $\Delta(O_2/Ar)$ of 1.8 ± 0.3 % were observed on April 25th 2015.

Largest variations in $^{17}\Delta$ and $\Delta(O_2/Ar)$ were observed within the thermocline. In October 2013, the $^{17}\Delta$ gradually increased with depth to a maximum of 182 per meg at 80 m, and then decreased (Fig. 4a). On the 5th of August 2014, the highest $^{17}\Delta$ values reached 218 per meg at 100 m (Fig. 4b). The depth trend on the 6th fairly resembled the one from the 5th, but the $^{17}\Delta$ values between the two days varied up to 61 per meg at 150 m. In April 2015, the $^{17}\Delta$ variations were comparatively subtle, without a prominent sharp peak, ranging between 140 and 125 per meg in the upper 50 m to 150 m. A deep peak in $^{17}\Delta$ was observed at 600 m of 223 per meg (Fig. 4c).

4 Discussion

4.1 Seasonal trends in photosynthetic vs. atmospheric O$_2$ input in the upper water column

The combined approach of $^{17}\Delta$ and $\Delta(O_2/Ar)$ composition of dissolved O$_2$ has been shown to be a valuable tracer for distinguishing biologically mediated O$_2$ from that supplied by atmospheric air input to the euphotic zone (Luz et al., 1999; Luz and Barkan, 2000). This is because atmospheric O$_2$ has a unique isotopic signature generated by stratospheric photochemical reactions involving O$_3$, O$_2$, and CO$_2$ which fractionate its isotopes in a mass-independent way (e.g. see Lämmerzahl et al., 2002), while photosynthesis fractionates O$_2$ isotopes in a mass-dependant way. By definition, the atmospheric $^{17}\Delta_{atm} = 0$, although the air-water equilibrium $^{17}\Delta_{eq}$ deviates slightly from the atmospheric value ($^{17}\Delta_{eq} = 11 \pm 3$ per meg, see Section 2.1; Jurikova et al., 2016) due to fractionation at equilibrium where the $\delta^{17}O$ and $\delta^{18}O$ slopes (λ) during invasion and evasion follow a slope different to that of respiration. Marine photosynthesis increases the $^{17}\Delta$ of dissolved O$_2$ up to its maximum value of 250 per meg (the $^{17}\Delta$ of seawater), which indicates that the dissolved O$_2$ is completely of photosynthetic origin, while gas exchange with atmosphere drives the $^{17}\Delta$ back towards its equilibrium value. Respiration consumes O$_2$, but does not affect the relative proportion of $\delta^{17}O$ and $\delta^{18}O$, and hence the $^{17}\Delta$. Respiration may be traced by $\Delta(O_2/Ar)$ since O$_2$ and Ar are similarly affected by physical processes, but Ar does not have any biological sources and sinks. The coupling between $^{17}\Delta$ and $\Delta(O_2/Ar)$ thus serves as a powerful tool to monitor the photosynthetic vs. atmospheric influences on dissolved O$_2$.

The $\Delta(O_2/Ar)$ values for the October 2013 profile are unfortunately not available and we are limited to discussing the changes in dissolved O$_2$ content in context of the $^{17}\Delta$ data only. In comparison to the observations from August 2014 and April 2015, interestingly, during this month we observed considerably elevated $^{17}\Delta$ in the mixed layer (90 ± 28 per meg), implying the presence of biological O$_2$ (Table 1). High $^{17}\Delta$ values, such as the 122 per meg measured at 30 m depth seem particularly unusual, as any instantaneous increase in photosynthetic $^{17}\Delta$ signal in the mixed layer is expected to be limited due to continuous exchange with atmospheric O$_2$ and thus averaged against the background signal. It is also unlikely that these samples could have been affected by contamination, as any leak during the sampling or preparation would result in decreased $^{17}\Delta$ value due to influence from atmospheric O$_2$. A likely explanation for the observed high $^{17}\Delta$ would be the rather short O$_2$ production time (<1 day) against the relatively long residence time of O$_2$ in the mixed layer (12 days; see Section 2.2.), suggesting a sustained accumulation of biologically produced O$_2$. The timing of the high $^{17}\Delta$ values in the mixed layer (Fig.

10

4a) also coincided with the overall highest observed fluorescence in this study (Fig. 3a). The Chl−a maximum was situated below the mixed layer in the thermocline where we also recorded a $^{17}\Delta$ peak. The elevated mixed layer $^{17}\Delta$ values therefore

455 could also reflect transient increase in biological O_2 due to upward flux of photosynthetically produced dissolved O_2 from the Chl−a maximum horizon. In such a case the $^{17}\Delta$ and the primary production would also integrate O_2 from below the mixed layer, and may complicate the application of the steady state model. Assuming that these values really reflect the integrated O_2 production it may suggest rather high photosynthetic activity for an inter-monsoon period, probably enhanced by the onset of cooler temperatures after the summer.

460

The average mixed layer $^{17}\Delta$ and $\Delta(O_2/Ar)$ values from August 5th and 6th 2014 as well as from April 24th 2015 were, within the variations, indistinguishable from each (about 55 ± 13 per meg and -0.3 ± 0.4 %; Table 1). The observed $^{17}\Delta$ values reflect the presence of photosynthetic O_2, which based on the $\Delta(O_2/Ar)$ values was in near equilibrium concentrations to potentially slightly undersaturated (especially towards the bottom of the mixed layer if individual measurements are considered). Previous

465 studies have largely disregarded negative mixed layer $\Delta(O_2/Ar)$ values and attributed them to vertical mixing (Reuer et al., 2007; Stanley et al., 2010). During our sampling period we did not observe significant upwelling of water (internal wave) that could be indicative of diapycnal mixing and contribution from deeper water to the mixed layer, although data spanning the entire residence time of O_2 in the mixed layer would be needed for a more conclusive statement. Recently, Qin et al. (2021) reported $\Delta(O_2/Ar)$ from the northern slope of the SCS collected by continuous measurement of gases in the surface waters (5

470 m) during approximately 2 weeks in October 2014 and June 2015. While most of their values yielded positive $\Delta(O_2/Ar)$, the authors also reported negative values which they linked to upwelling caused by a localized cold eddy. Hence, it can be expected that vertical mixing would result in negative $\Delta(O_2/Ar)$ values at 5 m in the SCS which, however, was not observed in our data (our $\Delta(O_2/Ar)$ values at 5 m ranged between 0 to 1.6 %). Although some degree of exchange across the mixed layer boundary cannot be excluded, we postulate that at large our data reflects minimal photosynthetic activity characteristic of the summer

475 months at SEATS. This may be attributed to the strong seasonal thermal stratification and nutrient depletion (Wong et al., 2017b), as supported by the measured low fluorescence in August 2014 (Fig. 3b), in agreement with past observations (Liu et al., 2002).

Distinct $^{17}\Delta$ and $\Delta(O_2/Ar)$ values were observed on April 25th 2015 (~26 per meg and ~1.8 %; Table 1). Although the average

480 mixed layer signal from April 24th 2015 (52 ± 11 per meg and -0.5 ± 3.5 %) is more similar to the values from August 2014, if the deepest mixed layer sample from 20 m depth is removed from the calculation (despite still being situated within the mixed layer) the newly obtained mixed layer $\Delta(O_2/Ar)$ for April 24th 2015 would agree well with the values from April 25th 2015 (1.5 ± 0.2 %; with the $^{17}\Delta$ remaining unaffected 46 ± 7). This points towards variable conditions near the mixed layer boundary, potentially influenced by O_2 contribution from below waters where the $\Delta(O_2/Ar)$ was negative. The lower, closer to

485 equilibrium, $^{17}\Delta$ values on the second day of sampling indicate increased air-sea gas exchange rates, which drive oxygen production as evidenced by the elevated $\Delta(O_2/Ar)$ in the mixed layer (Fig. 4c). This is further supported by the intensified

11

fluorescence (Fig. 3c) and supersaturated dissolved oxygen waters (Fig. 3d) below the mixed layer. The distribution and
concentration of the deep chlorophyll maximum corresponds to characteristic monsoon-forced trends (Liu et al., 2002) and
demonstrates the vitality of the thermocline-dwelling phytoplankton and the important role of NEM winds on determining the
metabolic balance of the system. The overall lower $^{17}\Delta$ and $\Delta(O_2/Ar)$ values in the upper water column observed in April 2015
when compared to August 2014 (Fig. 4) may illustrate the extent of wind-induced vertical mixing, which could be sufficient
to reach the upper limit of the nutricline (e.g. Ning et al., 2004; Tseng et al., 2005) and supply nutrients to the phytoplankton
community. Similar $\Delta(O_2/Ar)$ values were also reported by Quin et al. (2021) for the slope region of the SCS and are typically
attributed to nutrients, especially nitrogen, becoming available to phytoplankton communities. Alternatively, between
February and April monsoon winds tend to carry minerals and iron rich dust particles from the deserts in Central Asia to the
northern SCS and SEATS (Lin et al., 2007; Duce et al., 1991; Fung et al., 2000), which loading could fuel the enhanced
biological production. These profiles thus serve as a good example of the local ecosystem interactions and underscore the close
dependence of the phytoplankton communities on the NEM forcing.

4.2 Primary production rates in South China Sea

Primary production, the synthesis of organic compounds from carbon-containing species is of critical importance to
biogeochemical cycling of carbon and oxygen that sustains the marine ecosystem. In a steady-state system we may distinguish
gross (GP) and net production (NP), where the former represents the total C fixed by primary producers and the latter the C
available to the heterotrophic community. The NP thus amounts to the difference between the GP and community respiration.
NP is positive when GP exceeds respiration and the ecosystem exports or stores organic C, while negative values result when
respiration exceeds GP and the ecosystem respires more organic C than it was able to produce. These terms are of fundamental
interest to ocean studies. However, their quantification is not straightforward, and thus far only limited information is available
globally and especially from SEATS and the SCS.

Our production rates are summarized in Table 1, derived from $\delta^{17}O$ and $\delta^{18}O$ values of dissolved oxygen using a steady-state
mixed layer oxygen budget model that allows for determining integrated productivity in the mixed layer over the residence
time of O_2 (as detailed in Section 2.2). We note that these estimates, however, do not account for complex physical processes
(vertical mixing, lateral advection) and non-steady state effects on the mass balance. Furthermore, as discussed in Section 2.2.
the choice of parametrisation method and approach for calculating gas exchange rates introduces uncertainties and merits a
careful consideration. The definition of the mixed layer depth is also highly relevant, although as shown both the temperature-
based and dissolved O_2-based definition resulted in similar depths in this study. We found that largest uncertainties on the
derived production rates (especially on the 16th October 2013 and on the 6th August 2014; Table 1) resulted from variations in
$\delta^{17}O$, $\delta^{18}O$ and $\Delta(O_2/Ar)$ between samples collected from a vertical profile through the mixed layer. These variations are
reported as the standard deviation of the mean composition of dissolved O_2 in the mixed layer, and are considered in the
calculation of our NP and GP rates.

We found comparable production rates on the two consecutive sampling days in August 2014, with mean GP about ~1500 mg C m^{-2} d^{-1}, and low NP rates averaging −13 mg C m^{-2} d^{-1}. Although these rates appear to indicate that the system metabolism was net heterotrophic, within the uncertainties (based on the Δ(O$_2$/Ar), δ^{17}O and δ^{18}O variations in the mixed layer) it was in net balance. Similar values and overall net (or close to net) balance likely prevails in the SCS during the SWM season, as with the exception of sporadic typhoon events, the environmental conditions can be expected to remain rather stable and the water column strongly stratified. The production was also within the errors comparable on April 24th 2015, yielding GP of about ~2000 mg C m^{-2} and NP of ~−40 mg C m^{-2} d^{-1}. On the second sampling day, April 25th, the GP was considerably lower (~600 mg C m^{-2} d^{-1}), and the NP higher (~140 mg C m^{-2} d^{-1}). This points towards a more dynamic system, likely influenced by the NEM conditions. It appears that the NEM forcing could shift the metabolism of the system from being close to net balance to net autotrophy, due to cooler temperatures and wind-induced mixing of the water column, providing nutrients from the subsurface waters into the mixed layer. Potentially, minor contribution to the signal could also come through the input of photosynthetically produced O$_2$ from below the mixed layer. Highest GP estimates were obtained in October 2013 of 6600 mg C m^{-2} d^{-1}, which is rather surprising since during inter-monsoon periods phytoplankton production is expected to be limited. The origin of the high GP rates in October 2013 appears related to the deeper mixed layer on this sampling day. Elevated ^{17}Δ values (122 per meg) were measured at 30 m, with some contribution to the signal potentially coming from the photic layer below. These estimates should therefore be treated with caution as diapycnal mixing across the base of the mixed layer, and/or heterogenous distribution of phytoplankton in the water column and potential in situ production at depth cannot be ruled out in which case the steady state no longer applies.

It is to be stressed that our estimates represent the mixed layer production rates rather than total water column rates. During our sampling campaigns at SEATS, the euphotic zone was persistently deeper (~30–70 m deeper) than the mixed layer (Table 1, Fig. 4). This may lead to underestimation of the true mixed layer NP values due to mixing or entrainment of low-O$_2$ waters into the mixed layer, and conversely overestimation of the true mixed layer GP values due to mixing or entrainment of high-^{17}Δ waters into the mixed layer, since the share of the production that takes place within the euphotic zone below the mixed layer cannot be accounted for by the present model. Nonetheless, it is likely that if respiration exceeds gross production in the mixed layer, and hence the NP is negative, the overall NP in the euphotic zone will also be negative, since deeper regions tend to have higher respiration rates. Thus, production estimates from paired ^{17}Δ and Δ(O$_2$/Ar) profiles are still useful for indicating trends in ecosystem metabolism, even on instances when the depths of the mixed and the euphotic layer differ. Our findings indicate that over the year respiration might be close to the GP, with phenomena such as the NEM forcing playing an important role in fuelling productivity. Hence, production during winters with cooler temperatures and windy days may play a decisive role determining the amount of organic C fixed. For instance, an oligotrophic system that is net heterotrophic most of the time could maintain overall net autotrophy with episodic production which occurs 10% of the time and is three times the background rate (Karl et al., 2003). Weakening of the East Asian Monsoon by anthropogenically induced global warming (e.g. Hsu and

13

Chen, 2002; Xu et al., 2006) is, however, likely to limit vertical transport and nutrient supply to the phytoplankton. It is to be seen to what extent this will affect the primary production and overall C balance at SEATS and SCS.

Previous primary production estimates from the SCS based on ^{14}C observations and modelling fall within the range of approximately 120–170 g C m^{-2} year^{-1} (Ning et al., 2004; Chen, 2005; Liu et al., 2002). Ning et al. (2004) studied seasonal patterns in phytoplankton and productivity, and based on ^{14}C bottle incubation experiments estimated the summer and winter daily production within the euphotic zone to be 390 ± 342 and 546 ± 409 mg C m^{-2} d^{-1}, respectively. Although the comparison between incubation-based ^{14}C productivity estimates and those derived from triple oxygen isotopes is not straightforward due to the different natures of the methods and temporal and spatial scales over which they integrate, it is important to attempt to place estimates in context of past observations. To convert ^{14}C production estimates from bottle incubations to GP we used a scaling factor 1.74 to correct for dark respiration and excretion of DO^{14}C (Hendricks et al., 2004). This gives mean summer to winter GP rates of approximately 680–950 mg C m^{-2} d^{-1} for the values reported by Ning et al. (2004). Omitting our high GP rates from October 2013 which are likely biased by mixed layer entrainment, this is lower than our mean rates of about 1410 ± 590 mg C m^{-2} d^{-1}. Similarly, previous attempts to compare the ^{14}C incubation-based and triple oxygen isotope-based estimates have generally found that the latter tends to overestimate the primary production by a factor of about 1–3 (Juranek and Quay, 2005; Quay et al., 2010; Juranek and Quay, 2013; Jurikova et al., 2016). Whether this is due to a high bias from the triple oxygen approach or a low bias from the bottle incubation method remains a matter of on-going debate, which only further measurements of marine productivity using both incubation-based and incubation-independent methods and comparison studies can resolve. We postulate that some of the high bias we found could be due to vertical mixing with deeper waters (which leads to higher $^{17}\Delta$). To a larger extent, the observed differences probably result from the low bias of the bottle incubation approach due to containment effects and/or missed infrequent episodes or patches of high productivity (Quay et al., 2010; Juranek and Quay, 2013) which are known to occur in the SCS. Much of our understanding and discussion of productivity in the SCS, however, remains limited by the availability of data, which at present likely only offers a snapshot of the full picture. Crucially, further measurements of primary productivity at an increased spatial and temporal resolution will provide a more comprehensive picture of production at SEATS and within the wider SCS, reduce the uncertainties involved and inform the discussion of methodological biases.

4.3 Comparison to other tropical time-series

Initially launched in 1998, and becoming part of the Joint Global Ocean Flux Study one year later (JGOFS; Shiah et al., 1999), the SEATS station has often been compared with the time series off Hawaii (the Hawaii Ocean Time-series, HOT), which together with the time series off Bermuda (the Bermuda Atlantic Time-series Study, BATS) were two key components of the former JGOFS program. In contrast to the typical features of tropical waters, characterized by minimal seasonal variations, and comparing to the low-latitude HOT station (Karl et al., 1996), the SEATS station located at an even lower latitude is characterised by a distinct phytoplankton biomass and primary production pattern (Tseng et al., 2005; Wong et al., 2007a).

14

690 This distinct pattern is largely governed by the East Asian Monsoon, which brings seasonal changes that affect the oceanography and biogeochemistry of the SCS (Chao et al., 1996a; Liu et al., 2002).

Our seasonal depth profiles from SEATS share some similarities with the tropical oligotrophic HOT station (Juranek and Quay, 2005), albeit with different $^{17}\Delta$ magnitudes. Notably, the $^{17}\Delta$ depth distribution pattern at SEATS was comparable to that at
695 HOT, with a broad summer $^{17}\Delta$ peak (above 200 per meg at 80 and 100 m depth) from August 2014 comparable to that at HOT during the same month (with values above 140 per meat at 120 and 150 m depth), as well as a high peak in October 2013 (above 180 per meg at 80 m) rather similar to that at HOT during October (above 140 per meg at 100 m). In February, the $^{17}\Delta$ values were overall much lower at HOT, reaching the highest values in the deep (above 90 per meg between 150 and 200 m). Possibly, such trends could also be expected for SEATS; in fact our data from April 2015 appears to bear a close resemblance
700 to this pattern, although a comparison of the same months would be preferable. Our maximum $^{17}\Delta$ values within the euphotic zone at SEATS (218 per meg at 100 m observed on 5th August 2014, Fig. 4b) are, however, to our knowledge much higher than any previously documented upper ocean values at HOT or elsewhere, which typically do not exceed ~160 per meg.

Obviating the estimates from October 2013, our GP and NP rates are comparable to those from HOT derived using the same
705 approach, where seasonal variation in GP and NP were in the range of 800–1470 mg C m^{-2} d^{-1} and –120 and 180 mg C m^{-2} d^{-1} (Juranek and Quay, 2005). Generally, we would, however, expect higher rates at SEATS, where both seasonal monsoon forcing and/or episodic typhoon events induce sufficient vertical mixing to bring nutrients to the mixed layer and stimulate primary production. Assuming that our rates present an underestimation of the productivity due to the relatively very shallow mixed layer, these differences could reconcile. Our observed variations in NP/GP (~–0.01 in August 2014, and between –0.02
710 and 0.23 in April 2015) also compare well with the seasonal trends reported from HOT (between –0.13 and 0.13 during summer and winter; Juranek and Quay, 2005) with tendency towards heterotrophy in the summer and autotrophy during winter months. Very low NP/GP ratios were also observed from other low latitude regions such as the Equatorial Pacific (Hendricks et al., 2005; Stanley et al., 2010). This supports the general parallels in ecosystem metabolism in the oligotrophic regions, but also given the broader variations in NP/GP ratios at SEATS, emphasizes the importance of the monsoon forcing on introducing
715 dynamics to this system.

4.4 New insights into the $^{17}\Delta$ in deep water

The $^{17}\Delta$ has been traditionally applied for evaluating primary production in the upper ocean, and thus far only little is known on the $^{17}\Delta$ composition of the deep ocean. Due to the conservative behaviour of O_2 in a parcel of deep water where it may no longer be influenced by air–sea gas exchange or photosynthesis, the $^{17}\Delta$ could also present a valuable tracer for deep water
720 mixing processes since any variations in $^{17}\Delta$ should principally result from mixing of waters with different $^{17}\Delta$ values. While respiration alone does not affect the tracer, the $^{17}\Delta$ may, however, behave non-conservatively and be altered by the combined effects of respiration and mixing. As shown by Nicholson et al. (2014) if two hypothetical parcels of water with very different

15

Deleted: it
Deleted: 3b
Deleted: (
Deleted:),
Deleted: based on δ-values
Deleted: fairly
Deleted: toward
Deleted: ,
Deleted: driving the
Deleted: of
Deleted:

$\delta^{17}O$ and $\delta^{18}O$ values (but same $^{17}\Delta$ values) mix; one with the starting composition of surface water and one that underwent a
735 Rayleigh fractionation until 5% of oxygen remained, the resulting $^{17}\Delta$ values can become negative. Subsurface (~100–300 m) measurements in the equatorial Pacific indeed reported few negative values (Hendricks et al., 2005). Measurements from deeper profiles (700 m) were carried out in the Gulf of Elat and showed that the $^{17}\Delta$ values below the thermocline varied considerably with seasons, a likely result of vertical as well as horizontal mixing (Wurgaft et al., 2013). In order to evaluate the behaviour of $^{17}\Delta$ in the deep water of SCS and its potential utility as a mixing tracer in an oceanographically very distinct
740 system, we measured the $^{17}\Delta$ composition of deep O_2 profiles (down to 3500 m depth) from SEATS.

An overview of the oceanography of SCS is available in Wong et al. (2007a). The subsurface water masses in SCS consist of three main water masses; 1) the Tropical Water situated at around 150 m originating from near the international dateline at 20–30 °N in the North Pacific (Suga et al., 2003), 2) the North Pacific Intermediate Water centred around 500 m with a source
745 in the subpolar regions in the North Pacific (You, 2003), and 3) the Deep Water below 2200 m. The Deep Water in the SCS basin is formed by Pacific water masses, which in the western Philippine Sea overflow the sill that separates it from the SCS. The characteristics of the deep water in the SCS are rather uniform and similar to those in the western Philippine Sea, maintained by a mass balance between the inflowing deep water from the Phillipine Sea, upwelling and mixing with the shallower North Pacific Intermediate Water, and outflow at an intermediate depth through the Luzon Strait (Gong et al, 1992;
750 Chao et al., 1996b; Hu et al., 2000).

Our data showed overall elevated $^{17}\Delta$ values (>140 per meg) below 200 m depth for both August 2014 and April 2015 profiles. Largest variations were found at 200 m with a decrease of 116 per meg from August 2014 to April 2015 (Fig. 5a), coinciding with changes in the temperature-salinity characteristics of the Tropical Water mass (Fig. 5b). The synergic decrease in $^{17}\Delta$ and
755 increase in temperature-salinity at this depth illustrate the increased winter inflow of water to the SCS from Kuroshio through the Luzon Strait, or possibly also partially from the East China Sea through the Taiwan Strait (Fig. 1). This highlights the importance of NEM winds on driving the seasonal circulation inducing vertical mixing, which extends down to 400 m and leads to a full exchange of water masses during a winter (Fig. 5a). Historic records also support intrusions of North Pacific water masses to the SCS all year around with greatest strength in winter (Qu et al., 2000). Below, the deeper water remained
760 relatively homogenous, and did not appear to be influenced by seasonal changes, marking the limit of the extent of monsoon-driven circulation influence on the mixing. Surprisingly, variations in $^{17}\Delta$ (around ~20 per meg) were found beneath the thermocline base, however, considering the low O_2 content at these depths, even a very minor change in O_2 concentration may result in a large effect on the $^{17}\Delta$ signal. Although further observations from the SCS are needed for a more comprehensive picture, our first results advocate for the $^{17}\Delta$ as a valuable tracer of mixing processes, which brings new insights into some of
765 the key aspects of our understanding of the circulation in SCS.

5 Conclusions

In summary, in this study we provided the first insights into the $^{17}\Delta$ composition of dissolved O_2 at the SEATS station and within the South China Sea (SCS). We used the combined $^{17}\Delta$ and $\Delta(O_2/Ar)$ approach to monitor the seasonal changes in atmospheric vs. photosynthetic O_2 input to the upper part of the ocean, and to calculate the integrated mixed layer GP and NP rates. Our results showed that the net biological production at SEATS was negligible during most sampling days and close to net zero, but increased when the system was more dynamic during a spring influenced by the northeast monsoon forcing. Mixed layer variations and potential O_2 contribution from below the mixed layer, however, contribute uncertainties to these estimates and should be taken into consideration in further work applying this tracer, in particular within the SCS. Furthermore, we found the $^{17}\Delta$ of the deep water a promising tracer for physical mixing process (in addition to biological processes). This permitted us to evaluate the extent of the basin-wide monsoon-driven circulation in the water column and at depth, as well as to revisit the deep mixing processes. Although further work is required before the deep $^{17}\Delta$ may be confidently applied as a tracer of water mass mixing, our study showed that it could bring new perspectives on the renewal rate of the deep water, at least within the SCS. Thus, further deep $^{17}\Delta$ measurements within the region but also globally would be desirable. Similarly, further $^{17}\Delta$ and $\Delta(O_2/Ar)$ measurements within the SCS at an increased spatio-temporal resolution would be beneficial for gaining a more comprehensive picture of primary productivity dynamics at SEATS and its link and responses to the East Asian Monsoon as well as other episodic or interannual phenomena.

Data availability

The data used in this study is available in the accompanying Supplement including geochemical data (Table S1 and S2), CTD data (Table S3), and wind speed data (Table S4).

References

Barkan E. and Luz B.: High-precision measurements of $^{17}O/^{16}O$ and $^{18}O/^{16}O$ of O_2 and O_2/Ar ratio in air. Rapid Communication in Mass Spectrometry 17, 2809–2814, https://doi.org/10.1002/rcm.1267, 2003.

17

Benson B. B. and Krause Jr. D. K.: The concentration and isotopic fractionation of oxygen dissolved in freshwater and seawater in equilibrium with the atmosphere. Limnology and Oceanography 29, 620–632, https://doi.org/10.4319/lo.1984.29.3.0620, 1984.

Cai W.-J. and Dai M.: Comment on ''Enhanced open ocean storage of CO_2 from shelf sea pumping''. Science 306, 1477, https://doi.org/10.1126/science.1102132, 2004.

Castro-Morales K. and Kaiser J.: Using dissolved oxygen concentrations to determine mixed layer depths in the Bellingshausen Sea. Ocean Science 8, 1–10, https://doi.org/10.5194/os-8-1-2012, 2012.

Castro-Morales K., Cassar N., Shoosmith D. R., and Kaiser J.: Biological production in the Bellingshausen Sea from oxygen-to-argon ratios and oxygen triple isotopes. Biogeosciences 10, 2273–2291, https://doi.org/10.5194/bg-10-2273-2013, 2013.

Chao S.-Y., Shaw P.-T., Wu S.S.: El Niño modulation of the South China Sea circulation. Progress in Oceanography 38, 51–93, https://doi.org/10.1016/S0079-6611(96)00010-9, 1996a.

Chao S.-Y., Shaw P.-T., Wu S.S.: Deep water ventilation in the South China Sea. Deep-Sea Research I 43, 445–466, https://doi.org/10.1016/0967-0637(96)00025-8, 1996b.

Chen C.-C., Shiah F.-K., Chung S.-W., Liu K.-K.: Winter phytoplankton blooms in the shallow mixed layer of the South China Sea enahnced by upwelling. Journal of Marine Systems 59, 97–110, https://doi.org/10.1016/j.jmarsys.2005.09.002, 2006.

Chen C.-T. A., Liu K.-K.., Macdonald R.: Continental margin exchanges, in Ocean Biogeochemistry: The Role of the Ocean Carbon Cycle in Global Change. Edited by M. J. R. Fasham, Springer, New York, 53–98, https://doi.org/10.1007/978-3-642-55844-3_4, 2003.

Chen, Y. L.: Spatial and seasonal variations of nitrate-based new production and primary production in the South China Sea. Deep-Sea Research I 52, 319–340, https://doi.org/10.1016/j.dsr.2004.11.001, 2005.

Carr M.-E., et al.: A comparison of global estimates of marine primary production from ocean color. Deep-Sea Research II 53, 741–770, https://doi.org/10.1016/j.dsr2.2006.01.028, 2006.

855   Duce R.A., et al. The atmospheric input of trace species to the world ocean. Global Biogeochemical Cycles 5, 193–259, https://doi.org/10.1029/91GB01778, 1991.

DeGrandpre M.D., Olbu G.J., Beatty C.M., Hammar T.R.: Air-CO_2 fluxes on the US Middle Atlantic Bight. Deep Sea Research Part II: Topical Studies in Oceanography 49, 4355–4367, https://doi.org/10.1016/S0967-0645(02)00122-4, 2002.

860

Emerson S., Quay P. D., Stump C., Wilbur D., and Schudlich R.: Chemical tracers of productivity and respiration in the subtropical Pacific Ocean. Journal of Geophysical Research: Oceans 100, 15873–15887, https://doi.org/10.1029/95JC01333, 1995.

865   Frankignoulle M. and Borges A.V.: European continental shelf as a significant sink for atmospheric carbon dioxide. Global Biogeochemical Cycles 15, 569–576, https://doi.org/10.1029/2000GB001307, 2001.

Fung I.Y., Meyn S.K., Tegen I., Doney S.C., John J.G., Bishop J.K.B.: Iron supply and demand in the upper ocean. Global Biogeochemical Cycle 14, 281–296, https://doi.org/10.1029/1999GB900059, 2000.

870

Gong G.-C., Liu K.K., Liu C.-T., and Pai S.-C.: The chemical hydrography of the South China Sea west of Luzon and a comparison with the West Philippine Sea. TAO 3, 587-602, https://doi.org/10.3319/TAO.1992.3.4.587(O), 1992.

Gong G.-C., Chen Y.-L. L., and Liu K.-K.: Chemical hydrography and chlorophyll a distribution in the East China Sea in 875   summer: implications in nutrient dynamics. Cont. Shelf Res. 16, 1561–1590. https://doi.org/10.1016/0278-4343(96)00005-2, 1996.

Hamme R. C., Cassar N., Lance V. P., Vaillancourt R. D., Bender M. L., Strutton P. G., Moore T. S., DeGrandpre M. D., Sabine C. L., Ho D. T., and Hargreaves B. R.: Dissolved O_2/Ar and other methods reveal rapid changes in productivity during 880   a Lagrangian experiment in the Southern Ocean. Journal of Geophysical Research 117, C00F12, https://doi.org/10.1029/2011JC007046, 2012.

Hendricks M.B., Bender M.L., Barnett B.A.: Net and gross O_2 production in the Southern Ocean from measurements of biological O_2 saturation and its triple isotope composition. Deep Sea Research Part I: Oceanographic Research Papers 51, 885   https://doi.org/10.1016/j.dsr.2004.06.006, 1541–1561, 2004.

19

Hendricks M.B., Bender M.L., Barnett B.A., Strutton P., Chavez F.P.: Triple oxygen isotope composition of dissolved O_2 in the equatorial Pacific: A tracer of mixing, production, and respiration. Journal of Geophysical Research 110, C12021, https://doi.org/10.1029/2004JC002735, 2005.

890

Hu J., Kawamura H., Hong H., and Qi Y.: A Review on the Currents in the South China Sea: Seasonal Circulation, South China Sea Warm Current and Kuroshio Intrusion. Journal of Oceanography 56, 607–624, https://doi.org/10.1023/A:1011117531252, 2000.

895 Hsu H.-H. and Chen C.-T.: Observed and projected climate change in Taiwan. Meteorology and Atmospheric Physics 79, 87–104, https://doi.org/10.1007/s703-002-8230-x, 2002.

Juranek L.W. and Quay P.D.: In vitro and in situ gross primary and net community production in the North Pacific Subtropical Gyre using labelled and natural abundance isotopes of dissolved O_2. Global Biogeochemical Cycles 19, GB30009,
900 https://doi.org/10.1029/2004GB002384, 2005.

Juranek L. W. and Quay P. D.: Using triple isotopes of dissolved oxygen to evaluate global marine productivity. Annual Review of Marine Science 5, 503–524, https://doi.org/10.1146/annurev-marine-121211-172430, 2013.

905 Juranek L. W., Quay P. D., Feely R. A., Lockwood D., Karl D. M., and Church M. J.: Biological production in the NE Pacific and its influence on air-sea CO_2 flux: Evidence from dissolved oxygen isotopes and O_2/Ar. Journal of Geophysical Research 117, C05043, https://doi.org/10.1029/2011JC007450, 2012.

Jurikova H., Guha T., Abe O., Shiah F.-K., Wang C.-H., and Liang M.-C.: Variations in triple isotope composition of dissolved
910 oxygen and primary production in a subtropical reservoir. Biogeosciences 13, 6683–6698, https://doi.org/10.5194/bg-13-6683-2016, 2016.

Kaiser J., Reuer M. K., Barnett B., and Bender M. L.: Marine productivity estimates from O_2/Ar ratio measurements by membrane inlet mass spectrometry. Journal of Geophysical Research 32, L19605, https://doi.org/10.1029/2005GL023459,
915 2005.

Kaiser J.: Technical note: Consistent calculation of aquatic gross production from oxygen triple isotope measurements. Biogeosciences 8, 1793–1811, https://doi.org/10.5194/bg-8-1793-2011, 2011.

20

Karl D.M. and Lukas R.: The Hawaii Ocean Time-series (HOT) program: Background, rationale and field implementation. Deep Sea Research Part II: Topical Studies in Oceanography 43, 129–156, https://doi.org/10.1016/0967-0645(96)00005-7, 1996.

Karl D.M., Laws E.A., Morris P., Williams P.J.L.B., Emerson S.: Metabolic balance in the open sea. Nature 462, 32, https://doi.org/10.1038/426032a, 2003.

Lai C.-C., Wu C.-R., Chuang C.-Y., Tai J.-H., Lee K.-Y., Kuo H.-Y., and Shiah F.-K.: Phytoplankton and Bacterial Responses to Monsoon-Driven Water Masses Mixing in the Kuroshio Off the East Coast of Taiwan. Frontiers in Marine Science 8, 707807, https://doi.org/10.3389/fmars.2021.707807, 2021.

Laws E. A.: Photosynthetic quotients, new production and net community production in the open ocean. Deep-Sea Research I 38, 143– 167, https://doi.org/10.1016/0198-0149(91)90059-O, 1991.

Laws E. A., Landry M. R., Barber, R. T., Campbell L., Dickson M. L., and Marra J.: Carbon cycling in primary production bottle incubations: inferences from grazing experiments and photosynthetic studies using ^{14}C and ^{18}O in the Arabian Sea. Deep-Sea Research Part II, 47, 1339–1352, https://doi.org/10.1016/S0967-0645(99)00146-0, 2000.

Lämmerzahl P., Röckmann T., Brenninkmeijer C.A.M., Krankowsky D., Mauersberger K.: Oxygen isotope composition of stratospheric carbon dioxide. Geophysical Research Letters 29, 1582, https://doi.org/10.1029/2001GL014343, 2002.

Li H., Wiesner M.G., Chen J., Ling Z., Zhang J., Ran L.: Long-term variation of mesopelagic biogenic flux in the central South China Sea: Impact of monsoonal seasonality and mesoscale eddy. Deep-Sea Research Part I 126, 62−72, https://doi.org/10.1016/j.dsr.2017.05.012, 2017.

Lin I.-I., Liu W.T., Wu C.-C., Wong G.T.F., Hu C., Chen Z., Liang W.-D., Yang Y., and Liu K.-K.: New evidence for enhanced ocean primary production triggered by tropical cyclone. Geophysical Research Letters 30, 1718, https://doi.org/10.1029/2003GL017141, 2003.

Lin I.-I., Chen J.-P., Wong G.T.F., Huang C.-W., Lien C.-C.: Aerosol input to the South China Sea: Results from the MODerate Resolution Imaging Spectro-radiometer, the quick Scatterometer, and the Measurements of Pollution in the Troposphere Sensor. Deep-Sea Research Part II 54, 1589−1601, https://doi.org/10.1016/j.dsr2.2007.05.013, 2007.

Deleted: enhance

21

Lin I.-I., Lien C.-C., Wu C.-R., Wong G.T.F., Huang C.-W., Chiang T.-L.: Enhanced primary production in the oligotrophic
South China Sea by eddy injection in spring. Geophysical Research Letters 37, L16602,
https://doi.org/10.1029/2010GL043872, 2010.

Liang M.-C. and Mahata S. (2015) Oxygen anomaly in near surface carbon dioxide reveals deep stratospheric intrusion.
Scientific Reports 5, 11352, https://doi.org/10.1038/srep11352, 2015.

Liang M.-C., Mahata S., Laskar A.H., Thiemens M.H., and Newman S.: Oxygen isotope anomaly in tropospheric CO_2 and
implications for CO_2 residence time in the atmosphere and gross primary productivity. Scientific Reports 7,
https://doi.org/10.1038/s41598-017-12774-w, 2017.

Liu K.-K., Atkinson L., Chen C.T.A., Gao S., Hall J., MacDonald R.W., McManus L.T., Quiñones R.: Exploring continental
margin carbon fluxes on a global scale. EOS 81, 641–644, . https://doi.org/10.1029/EO081i052p00641-01, 2000.

Liu K.-K., Chao S.-Y., Shaw P.T., Gong G.-C., Chen C.-C., Tang T.Y.: Monsoon-forced chlorophyll distribution and primary
production in the South China Sea: observations and a numerical study. Deep-Sea Research Part I 49, 1387−1412,
https://doi.org/10.1016/S0967-0637(02)00035-3, 2002.

Lorenzen C.J.: Chlorophyll b in the eastern North Pacific Ocean. Deep-Sea Research 28A, 1049–1056,
https://doi.org/10.1016/0198-0149(81)90017-0, 1981.

Luz B. and Barkan E.: Assessment of Oceanic Productivity with the Triple-Isotope Composition of Dissolved Oxygen. Science
288, 2028–2031, https://doi.org/ 10.1126/science.288.5473.2028, 2000.

Luz B. and Barkan E.: The isotopic ratios $^{17}O/^{16}O$ and $^{18}O/^{16}O$ in molecular oxygen and their significance in biogeochemistry.
Geochimica et Cosmochimica Acta 69, 1099–1110, https://doi.org/10.1016/j.gca.2004.09.001, 2005.

Luz B., Barkan E., Bender M. L., Thiemens M. H., and Boering K. A.: Triple-isotope composition of atmospheric oxygen as
a tracer of biosphere productivity. Nature 400, 547–550, https://doi.org/10.1038/22987, 1999.

Luz B., Barkan E., Sagi Y., and Yacobi Y. Z.: Evaluation of community respiratory mechanisms with oxygen isotopes: A case
study in Lake Kinneret. Limnology and Oceanography 47, 33–42, https://doi.org/10.4319/lo.2002.47.1.0033, 2002.

Deleted: prpduction

Luz B., and Barkan E.: Proper estimation of marine gross O_2 production with $^{17}O/^{16}O$ and $^{18}O/^{16}O$ ratios of dissolved O_2. Geophysical Research Letters 38, L19606, https://doi.org/10.1029/2011GL049138, 2011.

990

Mahata S., Bhattacharya S.K., Wang C.-H., and Liang M.-C.: An improved CeO_2 method for high-precision measurements of $^{17}O/^{16}O$ ratios for atmospheric carbon dioxide. Rapid Communications in Mass Spectrometry 26, 1909–1922, https://doi.org/10.1002/rcm.6296, 2012.

995 Marra J.: Approaches to the measurement of plankton production, Phytoplankton productivity: carbon assimilation in marine and freshwater ecosystem. Edited by Willams P. J. le B., Thomas D. N., and Reynolds C. S. Cambridge, Blackwells, 78–108, https://doi.org/10.1002/9780470995204.ch4, 2002.

Nicholson D., Stanley R. H. R., and Doney S. C.: The triple oxygen isotope tracer of primary productivity in a dynamic ocean
1000 model: Triple oxygen isotopes in a global model. Global Biogeochemical Cycles, 28, 538–552. https://doi.org/10.1002/2013GB004704, 2014.

Ning X., Chai F., Xue H., Cai Y., Liu C., and Shi J.: Physical-biological oceanographic coupling influencing phytoplankton and primary production in the South China Sea. Journal of Geophysical Research 1009, C10005,
1005 https://doi.org/10.1029/2004JC002365, 2004.

Pai S. C., Gong G. C., and Liu K. K.: Determination of dissolved oxygen in seawater by direct spectrophotometry of total iodine. Marine Chemistry 41, 343–351, https://doi.org/10.1016/0304-4203(93)90266-Q, 1993.

1010 Prokopenko M. G., Pauluis O. M., Granger J., and Yeung L. Y.: Exact evaluation of gross photosynthetic production from the oxygen triple-isotope composition of O_2: Implications for the net-to-gross primary production ratios. Geophysical Research Letters 38, L14603, https://doi.org/10.1029/2011GL047652, 2011.

Qin C., Zhang G., Zheng W., Han Y., Liu S.: High-resolution distributions of O_2/Ar on the northern slope of the South China
1015 Sea and estimates of net community production. Ocean Scince 17, 249–264, https://doi.org/10.5194/os-17-249-2021.

Qu T., Mitsudera H., Yamagata T.: Intrusion of the North Pacific waters into the South China Sea. Journal of Geophysical Research 105, 6415–6424, https://doi.org/10.1029/1999JC900323, 2000.

1020 Qu T., Du Y., Meyers G., Ishida A., Wang. D.: Connecting the tropical Pacific with Indian Ocean through South China Sea. Geophysical Research Letters 32, L24609, https://doi.org/10.1029/2005GL024698, 2005.

23

Quay P.D., Peacock C., Björkman K., Karl D.M.: Measuring primary production rates in the ocean: Enigmatic results between incubation and non-incubation methods at Station ALOHA. Global Biogeochemical Cycles 24, GB3014, https://doi.org/10.1029/2009GB003665, 2010.

Regaudie-de-Gioux A., Lasternas S., Augustí S., and Duarte C.M.: Comparing marine primary production estimates through different methods and development of conversion equations. Frontiers in Marine Science 1, 19, https://doi.org/10.3389/fmars.2014.00019, 2014.

Rehder G. and Suess E.: Methane and pCO_2 in the Kuroshio and the South China Sea during maximum summer surface temperatures. Marine Chemistry 75, 89–108, https://doi.org/10.1016/S0304-4203(01)00026-3, 2001.

Reuer M.K., Barnett B.A., Bender M.L., Falkowski P.G., Hendricks M.B.: New estimates of Southern Ocean biological production rates from O_2/Ar ratios and the triple isotope composition of O_2. Deep Sea Research I 54, 951–974, https://doi.org/10.1016/j.dsr.2007.02.007, 2007.

Sarma V. V. S. S., Abe O., Hashimoto S., Hinuma A., and Saino T.: Seasonal variations in triple oxygen isotopes and gross oxygen production in the Sagami Bay, central Japan. Limnology and Oceanography 50, 544–552, https://doi.org/10.4319/lo.2005.50.2.0544, 2005.

Seguro I., Marca A.D., Painting S.J., Shutler J., Suggett D.J., and Kaiser J.: High-resolution net and gross biological production during a Celtic Sea spring bloom. Progress in Oceanography 177, 101885, https://doi.org/10.1016/j.pocean.2017.12.00, 2019.

Schlitzer R.: Ocean Data View, https://odv.awi.de/, 2020.

Shiah F.-K., Liu K.-K., Tang T.-Y.: South East Asian Time-series Station established in South China Sea. US JGOFS Newsletter 10 , 8–9, 1999.

Stanley R. H. R., Kirkpatrick J. B., Cassar N., Barnett B. A., and Bender M. L.: Net community production and gross primary production rates in the western equatorial Pacific. Global Biogeochemical Cycles 24, GB4001, https://doi.org/10.1029/2009GB003651, 2010.

Steeman-Nielsen E.: The use of radioactive carbon (^{14}C) for measuring organic production in the sea. ICES Journal of Marine Science (Journal du Conseil) 18, 117–140, https://doi.org/10.1093/icesjms/18.2.117, 1952.

24

Strickland J.D.H and Parsons T.R.: A Practical Handbook of Seawater Analysis. Bulletin 167 (Second Edition) Fisheries Research Board of Canada, Ottawa, 1972.

1060 Shang S., Zhang C., Hong H., Liu Q., Wong G.T.F., Hu C., and Huang B.: Hydrographic and biological changes in the Taiwan Strait during the 1997–1998 El Niño winter. Geophysical Research Letters 32, L11601, https://doi.org/10.1029/2005GL022578, 2005.

Suga T., Kato A., Hanawa K.: North Pacific Tropical Water: its climatology and temporal changes associated with the climate
1065 regime shift in the 1970s. Progress in Oceanography 47, 223–256, https://doi.org/10.1016/S0079-6611(00)00037-9, 2003.

Tai J.-H., Wong G.T.F., and Pan X. Upper water structure and mixed layer depth in tropical waters: The SEATS station in the northern South China Sea. Terrestrial, Atmospheric, and Oceanic sciences journal 28, 1019–1032, https://doi.org/10.3319/TAO.2017.01.09.01, 2017.
1070
Tai J.-H., Chou W.-C., Hung C.-C., Wu K.-C., Chen Y.-H., Chen T.-Y., Gong G.-C., Shiah F.-K., and Chow C. H.: Short-term variability of biological production and CO_2 system around Dongsha Atoll of the northern South China Sea: Impact of topography-flow interation. Frontiers in Marine Sciences 7, 511, https://doi.org/10.3389/fmars.2020.00511, 2020.

1075 Thomas H., Bozec Y., Elkalay K., de Baar H.J.W.: Enhanced Open Ocean Storage of CO_2 from Shelf Sea Pumping. Science 304, 1005–1008, https://doi.org/10.1126/science.1095491, 2004.

Tseng C.-M., Wong G.T.F., Lin I.-I., Wu C.-R., and Liu K.-K.: A unique seasonal pattern in phytoplankton biomass in low-latitude waters in the South China Sea. Geophysical Research Letters 32, L08608, https://doi.org/10.1029/2004GL022111,
1080 2005.

Tseng C.-M., Wong G.T.F., Chou W.-C., Lee B.-S., Sheu D.-D., Liu K.-K.: Temporal variations in the carbonate system in the upper layer at the SEATS. Deep-Sea Research II 54, 1448–1468, https://doi.org/10.1016/j.dsr2.2007.05.003, 2007.

1085 Tseng C.-M., Liu K.-K., Wang L.-W., Gong G.-C.: Anomalous hydrographic and biological conditions in the northern South China Sea during the 1997-1998 El Niño and comparisons with the equatorial Pacific. Deep-Sea Research I 56, 2129–2143, https://doi.org/10.1016/j.dsr.2009.09.004, 2009.

25

Tsunogai S., Watanabe S., and Sato T.: Is there a "continental shelf pump" for the absorption of atmospheric CO_2? Tellus 51, 701−712, https://doi.org/10.1034/j.1600-0889.1999.t01-2-00010.x, 1999.

Wang S.-L., Chen C.-T.A., Hong G.-H., and Chung C.-S.: Carbon dioxide related parameters in the East China Sea. Continental Shelf Research 2000, 525–544, https://doi.org/10.1016/S0278-4343(99)00084-9, 2000.

Wanninkhof R., Asher W. E., Ho D. T., Sweeney C., and McGillis W. R.: Advances in quantifying air-sea gas exchange and environmental forcing. Annual Review of Marine Science 1, 213–244, https://doi.org/10.1146/annurev.marine.010908.163742, 2009.

Wong G.T.F., Ku T.-L., Mulholland M., Tseng C.M., and Wang D.-P.: The SouthEast Asian Time-series Study (SEATS) and the biogeochemistry of the South China Sea – An overview. Deep-Sea Research Part II 54, 1434−1447, https://doi.org/10.1016/j.dsr2.2007.05.012, 2007a.

Wong G.T.F., Tseng C.-M., Wen L.-S., and Chung S.-W.: Nutrient dynamics and N-anomaly at the SEATS station. Deep-Sea Research Part II 54, 1528–1545, https://doi.org/10.1016/j.dsr2.2007.05.011, 2007b.

Wurgaft E., Shamir O., Barkan E., Paldor N., and Luz B.: Mixing processes in the deep water of the Gulf of Elat (Aqaba): evidence from measurements and modelling of the triple isotopic composition of dissolved oxygen. Limnology and Oceanography 58, 1373−1386, https://doi.org/10.4319/lo.2013.58.4.1373, 2013.

Xu M., Chang C.-P., Fu C., Qi Y., Robock A., Robinson D., and Zhang H.-M.: Steady decline of east Asian monsoon winds, 1969–2000: Evidence from direct ground measurements of wind speed. Journal of Geophysical Research 111, D24111, https://doi.org/10.1029/2006JD00733, 2006.

Yool A. and Fasham M.J.R.: An examination of the "Continental shelf pump" in an open ocean general circulation model. Global Biogeochemical Cycles 15, 831–844, https://doi.org/10.1029/2000GB001359, 2001.

You Y.: The pathway and circulation of North Pacific Intermediate Water. Geophysical Research Letters 30, 2291, https://doi.org/10.1029/2003GL018561, 2003.

Zhai W., Dai M., Cai W.-J., Wang Y., Hong H.: The partial pressure of carbon dioxide and air-sea fluxes in the northern South China Sea in spring, summer and autumn. Marine Chemistry 96, 87–97, https://doi.org/10.1016/j.marchem.2004.12.002, 2005.

26

Zhou W. and Chan J. C. L.: ENSO and the South China Sea summer monsoon onset. International Journal of Climatology 27, 157–167, https://doi.org/10.1002/joc.1380, 2007.

125

Date	PLD[a]	MLD[b]	MLD[c]	C_o	K_{avg}	K_{wgh}	$\Delta(O_2/Ar)$	$^{17}\Delta$	NP	GP	NP / GP
	(m)	(m)	(m)	(mmol m^{-3})	(m d^{-1})	(m d^{-1})	(%)	(per meg)	(mg C m^{-2} d^{-1})		
Oct. 16th, 2013	81	49	48	201.29	4.0	6.4	–	90 ± 28	–	6660 ± 2930	–
Aug. 5th, 2014	77	25	20	198.04	4.7	3.2	–0.3 ± 0.5	59 ± 9	–18 ± 27	1620 ± 170	–0.01
Aug. 6th, 2014	79	34	32	198.04	4.7	3.2	–0.2 ± 0.2	54 ± 18	–8 ± 13	1400 ± 530	–0.01
Apr. 24th, 2015	101	28	27	204.63	5.7	4.7	–0.5 ± 3.5	52 ± 11	–43 ± 283	2010 ± 720	–0.02
Apr. 25th, 2015	101	26	25	204.63	5.7	4.7	1.8 ± 0.3	26 ± 5	143 ± 24	620 ± 250	0.23

[a]Photic layer depth. [b]Temperature-based mixed layer depth. [c]O_2-based mixed layer depth.

Table 1: Mixed-layer dissolved oxygen composition and estimated seasonal primary production rates at the SouthEast Asian Time-series Study (station 55, "SEATS") in the South China Sea (SCS) for October 2013, August 2014 and April 2015. NP and GP were calculated using the O_2-based mixed layer depth and weighted gas exchange rate (K_{wgh}). The GP and NP uncertainties are based on $\Delta(O_2/Ar)$, $\delta^{17}O$ and $\delta^{18}O$ variations between dissolved O_2 samples collected from a vertical profile through the mixed layer (1σ of the mean, n = 3 for each sampling day).

130

28

Figure 1: Bathymetric map of South China Sea (SCS) and surrounding areas with position of the SouthEast Asian Time-series Study (station 55, "SEATS") indicated. Arrows in SCS indicate the circulation patterns – solid line shows the basin-wide cyclonic gyre during winter, dashed line represents the eastward jet off the Vietnam coast and the anticyclonic gyre over the southern half of the SCS throughout the summer. Map was created using Ocean Data View (https://odv.awi.de/; Schlitzer, 2020).

180
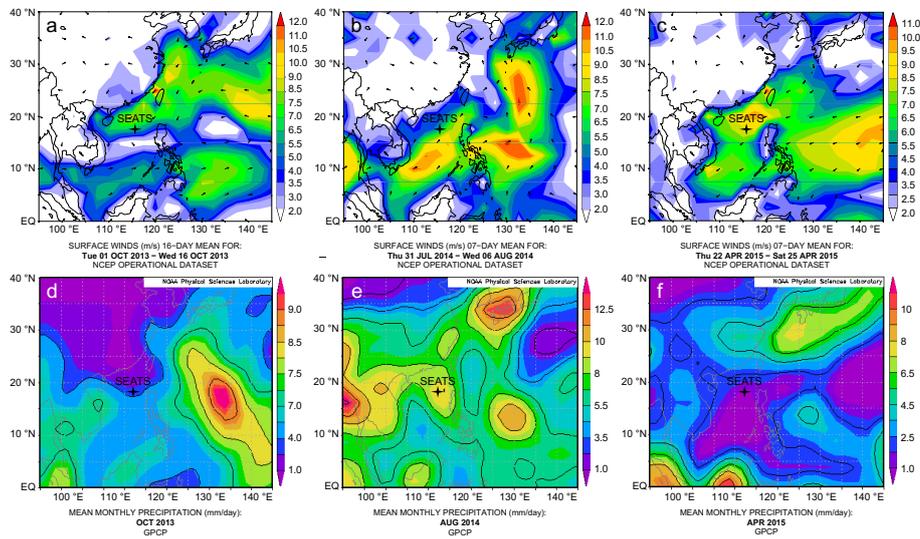
Figure 2: Upper panels – surface vector wind maps indicating the monsoon seasons: a) inter-monsoon period in October 2013; b) southwest summer monsoon in August 2014; c) northeast winter monsoon in April 2015. Lower panels – mean monthly precipitation: d) in October 2013; e) in August 2014; c) and in April 2015. Maps of vector wind distributions were obtained from the NOAA – Atmospheric Variables Plotting Page using the NCEP daily analysis data (https://www.esrl.noaa.gov/psd/data/histdata/). Maps of precipitation were obtained from NOAA's GPCP Version 2.3 Combined Precipitation Data Set (https://psl.noaa.gov/data/gridded/data.gpcp.html).

1185
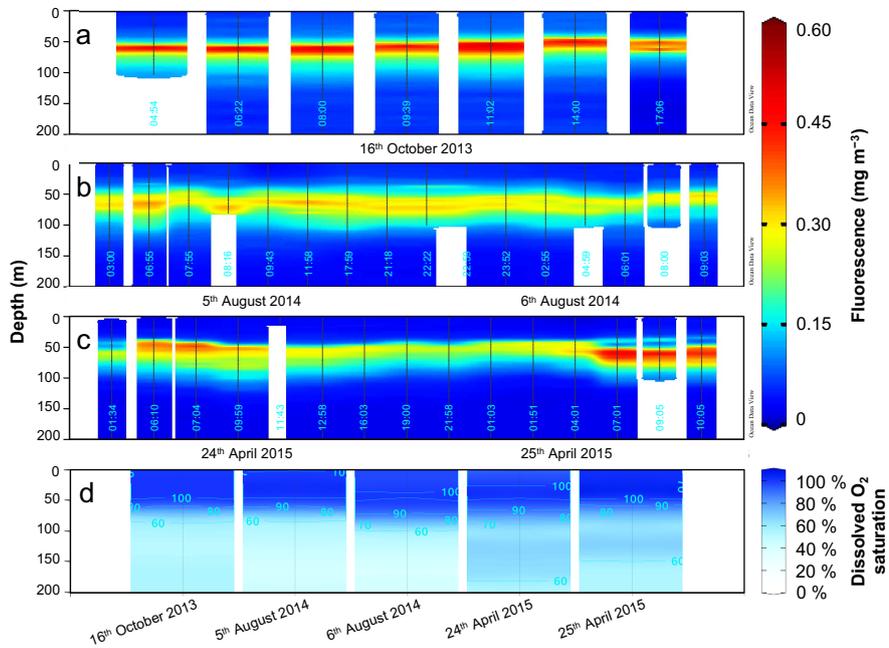
Figure 3: Fluorescence (mg m⁻³) time-series from SEATS on: a) 16ᵗʰ October 2013; b) 5ᵗʰ–6ᵗʰ August 2014 and; c) 24ᵗʰ–25ᵗʰ April 2015). d) Depth profiles of dissolved O₂ saturation (%) during the different sampling days, calibrated to manual dissolved O₂ measurements. Data visualisation was done using Ocean Data View (https://odv.awi.de/; Schlitzer, 2020).

October 2013

August 2014

April 2015

a

b

c

$^{17}\Delta$ (per meg, vs. air)

$^{17}\Delta$ (per meg, vs. air)

$^{17}\Delta$ (per meg, vs. air)

Depth (m)

Temperature (°C)

Temperature (°C)

Temperature (°C)

$\Delta(O_2/Ar)$ (%, vs. air)

$\Delta(O_2/Ar)$ (%, vs. air)

MLD

PLD

Thermocline base limit

— Aug. 5th, 2014
○— Aug. 6th, 2014
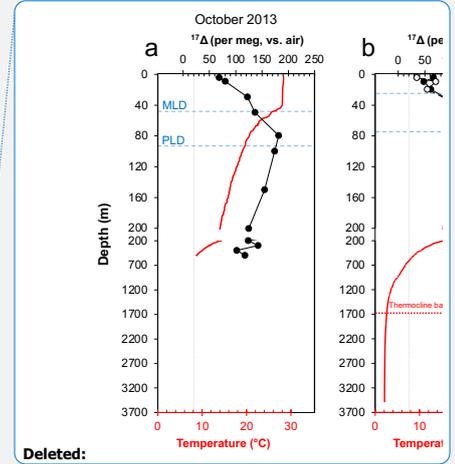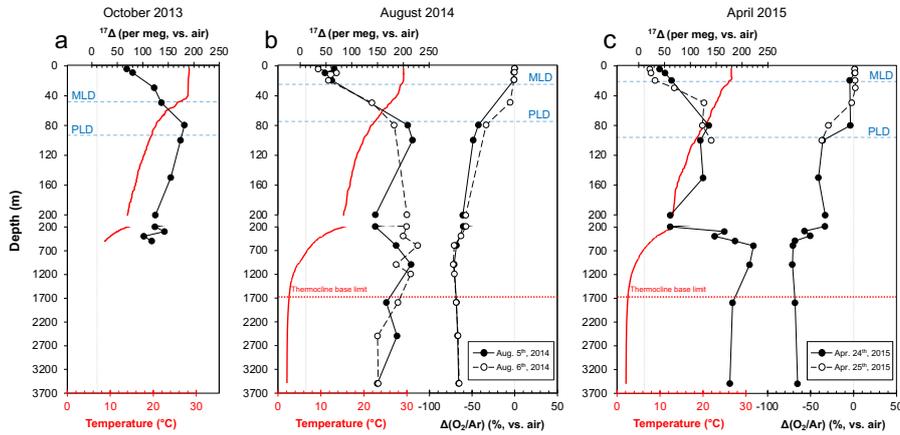
— Apr. 24th, 2015
○— Apr. 25th, 2015

Figure 4: Depth profiles of temperature (red lines) and $^{17}\Delta$ and $\Delta(O_2/Ar)$ profiles (solid or dashed black lines) from SEATS from: a) 16th October 2013 (inter-monsoon season); b) 5th–6th August 2014 (summer southwest monsoon) and; c) 24th–25th April 2015 (winter northeast monsoon). Vertical dashed grey lines indicate the equilibrium $^{17}\Delta$ and $\Delta(O_2/Ar)$ values with atmosphere. MLD−mixed layer depth, PLD−photic layer depth.

32
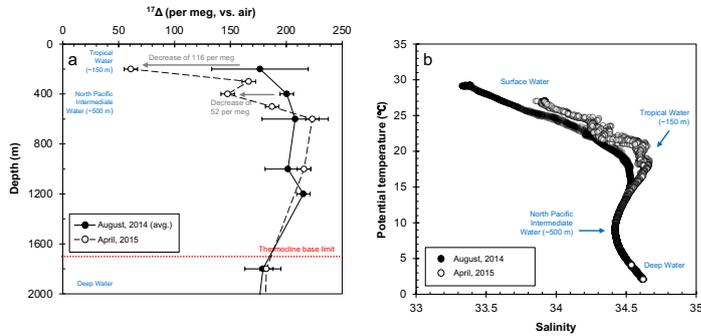
Figure 5: Deep water composition at SEATS from August 2014 to April 2015; a) ¹⁷Δ of dissolved O₂. The ¹⁷Δ values from August 2014 are shown as mean of the two sampling days (5th and 6th). Error bars indicate the standard deviation between the samples the two collection days (1σ) where available or the analytical uncertainty (6 per meg; 1σ). b) relationship between potential temperature and salinity. Salinity peak of ~34.6 (and ~20 °C) corresponds to the Tropical Water situated around 150 m, while the minimum of ~34.4 indicates the North Pacific Intermediate Water at around 500 m. The Deep Water below the thermocline base (~1700 m) is characterised by low temperatures ~2 °C and high salinities around ~34.6.

33

Page 28: [1] Formatted   HJ   15/02/2022 01:23:00

Left

Page 28: [2] Formatted   HJ   15/02/2022 01:23:00

English (UK)

Page 28: [3] Formatted   HJ   15/02/2022 01:23:00

Font colour: Auto

Page 28: [4] Formatted   HJ   15/02/2022 01:23:00

English (UK)

Page 28: [5] Merged Cells   HJ   15/02/2022 01:23:00

Merged Cells

Page 28: [6] Formatted   HJ   15/02/2022 01:23:00

Left, Line spacing: single

Page 28: [7] Deleted   HJ   15/02/2022 01:23:00

Page 28: [8] Formatted   HJ   15/02/2022 01:23:00

Left, Line spacing: single

Page 28: [9] Formatted   HJ   15/02/2022 01:23:00

English (UK)

Page 28: [10] Formatted   HJ   15/02/2022 01:23:00

English (UK)

Page 28: [11] Formatted   HJ   15/02/2022 01:23:00

Left, Line spacing: single

Page 28: [12] Formatted   HJ   15/02/2022 01:23:00

English (UK)

Page 28: [13] Formatted   HJ   15/02/2022 01:23:00

English (UK)

Page 28: [14] Formatted   HJ   15/02/2022 01:23:00

Left, Line spacing: single

Page 28: [15] Formatted   HJ   15/02/2022 01:23:00

English (UK)

Page 28: [16] Formatted   HJ   15/02/2022 01:23:00

English (UK)

Page 28: [19] Formatted   HJ   15/02/2022 01:23:00

English (UK)

Page 28: [20] Formatted   HJ   15/02/2022 01:23:00

Left, Line spacing: single

Page 28: [21] Formatted   HJ   15/02/2022 01:23:00

English (UK)

Page 28: [22] Formatted   HJ   15/02/2022 01:23:00

English (UK)

Page 28: [23] Deleted Cells   HJ   15/02/2022 01:23:00

Deleted Cells

Page 28: [24] Formatted   HJ   15/02/2022 01:23:00

Line spacing: single

Page 28: [25] Deleted   HJ   15/02/2022 01:23:00

Page 28: [25] Deleted   HJ   15/02/2022 01:23:00

Page 28: [25] Deleted   HJ   15/02/2022 01:23:00

Page 28: [25] Deleted   HJ   15/02/2022 01:23:00